Proceedings of IMECE04
2004 ASME International Mechanical Engineering Congress and Exposition
November 13-20, 2004, Anaheim, California USA

IMECE2004-59283

LIQUID WATER TRANSPORT IN POLYMER ELECTROLYTE FUEL CELLS WITH MULTI-LAYER DIFFUSION MEDIA

Ugur Pasaogullari, Chao-Yang Wang
Electrochemical Engine Center,
Department of Mechanical and Nuclear Engineering
The Pennsylvania State University
University Park, PA 16802 USA
Tel: +1-814-865-9768
Fax: +1-814-863-4848
E-mail: uyp101@psu.edu

Ken S. Chen
Engineering Sciences Center
Sandia National Laboratories
P.O. Box 5800, MS 0834
Albuquerque, NM 87185-0834 USA

ABSTRACT

A two-phase, multi-component, full cell model is developed in order to analyze the two-phase transport in polymer electrolyte fuel cells with multi-layer cathode gas diffusion media, consisting of a coarse gas diffusion layer (GDL) (average pore size ~10 μm) and a micro-porous layer (MPL) (average pore size ~0.2-2 μm). The relevant structural properties of MPL, including average pore size, wettability, thickness and porosity are examined and their effects on liquid water transport are discussed. It is found that MPL promotes back-flow of liquid water across the membrane towards the anode, consequently alleviating cathode flooding. Furthermore, it is seen that unique porous and wetting characteristics of MPL causes a discontinuity in the liquid saturation at MPL-GDL interface, which in turn reduces the amount of liquid water in cathode catalyst layer-gas diffusion medium interface in some cases. Our analyses show that the back-flow of liquid water increases with the increasing thickness and decreasing pore size, hydrophobicity and bulk porosity of the MPL.

Keywords: PEFC, flooding, GDL, micro-porous layer, two-phase transport, polymer electrolyte membrane

NOMENCLATURE

C^i Molar concentration of species i [mol·m^{-3}]
D_g Gas phase diffusion coefficient [m^2·s^{-1}]
d Average pore size [m]
F Faraday's constant [96487 C·mol^{-1}]
I Local current density [A·cm^{-2}]
j_m Mass flux [kg·m^{-2}·s^{-1}]
j_l Liquid flux [kg·m^{-2}·s^{-1}]
j_w Molar water flux [mol·m^{-2}·s^{-1}]
K Absolute permeability [m^2]
k_{rk} Relative permeability of phase k
M^i Molar weight of species i [kg·mol^{-1}]
n_d Electro-osmotic drag coefficient
p_c Capillary pressure [Pa]
s Liquid saturation
u Velocity [m·s^{-1}]
α Net water transport coefficient
δ_i Thickness of component i
ε Absolute porosity
γ_c Advection correction factor
λ Membrane water content (#H_3O^+/#SO_3^-)
λ_k Relative mobility of phase k
μ Dynamic viscosity [Pa·s]
ν Kinematic viscosity [m^2·s^{-1}]
ρ Density [kg·m^{-3}]

INTRODUCTION

One of the main limitations in polymer electrolyte fuel cell (PEFC) performance is governed by the transport of reactants to the catalyst layer, referred as mass transport limitation. This limitation is further increased by the presence of liquid water in the porous gas diffusion layer (GDL), which blocks some of the open pores and thus reduces the available path for transport of reactant species. This phenomenon is called flooding and it is most problematic in cathode due to the slower electrochemical kinetics of cathode oxygen reduction reaction. Lately, multi-layer gas diffusion media (GDM), consisting of a coarse GDL and a finer micro-porous layer (MPL) have been investigated to reduce the flooding in porous cathode and to enhance the water management of PEFCs by increasing tendency of back-flow of liquid water across the membrane towards anode. It has been

shown that highly hydrophobic MPLs usually exhibit better performance (Wilson *et al.* 1995, Qi and Kaufman 2002 and Kong *et al.* 2002). Although the exact mechanisms are yet to be fully elucidated, the performance enhancement is usually associated with better water management capabilities of MPLs. The two main effects of improvement with MPLs are due to enhancement of water management by better humidifying the membrane, consequently decreasing the ohmic losses and reducing the flooding in cathode, consequently improving the gas phase diffusion.

Although several studies have been carried out to model the two-phase transport in PEFCs, only a few has discussed the effects of MPL on water management and two-phase transport. Nam and Kaviany (2003) have modeled the two-phase transport in multi-layered cathode GDM using the unsaturated flow theory (UFT), which assumes the gas pressure in the GDL is constant, therefore neglects the gas flow counter to the liquid flow. They have optimized the MPL properties according to the total liquid water in the cathode GDM, and concluded that there is an optimum for thickness and porosity of the MPL. Most recently, Pasaogullari and Wang (2004a), elucidated the effect of MPL, using the more complete two-phase model *i.e.* M^2 formulation, which relaxes the constant gas phase pressure assumption, hence accounts for the gas flow counter to the capillarity-induced liquid flow. It was indicated for the first time that the build-up in liquid pressure in the cathode due to the presence of MPL creates a hydraulic pressure differential to drive water flow back to the anode. This water back flow can be controlled by the pore size and wettability of MPL following the capillary flow theory developed by Pasaogullari and Wang (2004b). In addition, the study of Pasaogullari and Wang (2004a) revealed a capillary-driven enhancement of oxygen transport once the two-phase zone is formed. This new enhancement mechanism is, however, over-dominated by the increase in the diffusion resistance, yielding an overall reduction in the oxygen transport limitation in most cases of flooding. In a meeting abstract, Weber and Newman (2003) also mentioned the positive role played by MPL to promote water back flow through the membrane, improving the humidification of the membrane as well as the anode catalyst layer, reducing the overall ohmic losses, hence improving the performance.

The aim of the present work is to present a two-phase flow model for the entire membrane-GDM assembly, based on the M^2 formulation (Wang and Cheng, 1997) and analyze the liquid water transport in PEFCs with MPLs. The effects of porous and wetting structure of MPL are also analyzed. The paper is organized as follows: The development of the mathematical model for multi-layered GDM and polymer electrolyte membrane (PEM) is presented based on the theory of liquid water flow in hydrophobic gas diffusion layers presented by Pasaogullari and Wang (2004a). Then, the liquid water transport with MPL is compared with the conventional PEFC configurations and the effects of MPL properties are examined.

MATHEMATICAL MODEL

The present study focuses on liquid water transport in porous gas diffusion anode and cathode and across the membrane. The cell is considered to be isothermal as a first approximation. The gas channels are excluded from the modeling domain by specifying boundary conditions at the gas diffusion media/channel interfaces. Furthermore, catalyst layers are taken to be infinitely thin; and hence the anode hydrogen oxidation reaction (HOR) and cathode oxygen reduction reaction (ORR) are assumed to take place at the PEM-GDM interfaces. Within these assumptions, the domain considered is confined to porous anode GDL, PEM and cathode GDM, consisting of MPL and GDL, as shown in Figure 1 along with the associated transport processes. Although the present model is developed in 1-D, it can be readily implemented in a multi-dimensional CFD model with the channel incorporated as shown in Pasaogullari and Wang (2004c).

In this study, the multi-phase, mixture model (M^2) is employed to describe the two-phase transport processes in the porous media. M^2 model is an exact reformulation of classical two-phase, two-fluid models into a single equation. Unlike the unsaturated flow theory (UFT) utilized in some of the earlier two-phase PEFC models (He *et al.* 2000 Nam and Kaviany 2003) M^2 model does not require the assumption of a constant gas phase pressure across the porous medium, hence it also accounts for the gas flow counter to the capillarity driven liquid flow. Furthermore, M^2 modeling does not require explicitly tracking of phase interfaces; consequently simplifies mathematical modeling of two-phase transport in porous medium, where both single- and two-phase regions coexist. The reader is referred to Wang and Cheng (1997) for details of the multiphase mixture model and its applications to a number of multiphase transport problems in porous media.

Mass conservation for the two-phase mixture in steady-state as given by M^2 formulation is:

$$\nabla \cdot (\rho \vec{u}) = 0 \tag{1}$$

In the above equation; $\vec{u}$ is the superficial mixture velocity and ρ is the mixture density and given as:

$$\rho = \rho_l \cdot s + \rho_g \cdot (1-s) \tag{2}$$

where s is the liquid saturation and represents the fraction of open pore space of porous media occupied by liquid.

When Eq. (1) is integrated along the GDM in steady-state:

$$\rho \vec{u} = \vec{j}_m \tag{3}$$

where $\vec{j}_m$ indicates the net mass flux through the porous media, and corresponding expressions for each individual layers are given in Table 1.

The species conservation equation of M^2 formulation, when written in terms of molar concentrations is (Pasaogullari and Wang, 2004a):

$$\nabla \cdot \left(\gamma_c \vec{u} C^i\right) = \nabla \cdot \left(D_g^{i,eff} \nabla C_g^i\right) - \nabla \cdot \left[\left(\frac{\mathrm{mf}_l^i}{M^i} - \frac{C_g^i}{\rho_g}\right)\vec{j}_l\right] \tag{4}$$

where the advection correction factor is:

$$\gamma_i = \begin{cases} \dfrac{\rho}{C^{\mathrm{H_2O}}}\left(\dfrac{\lambda_l}{M^{\mathrm{H_2O}}} + \lambda_g \dfrac{C_{sat}^{\mathrm{H_2O}}}{\rho_g}\right) & \text{for water} \\ \dfrac{\rho \lambda_g}{\rho(1-s)} & \text{for other species} \end{cases} \tag{5}$$

In Eq. (4), C^i denotes the total molar concentration of species i in liquid and gas phases, defined as:

$$C^i = (1-s)C_g^i + sC_l^i \tag{6}$$

The gas-phase diffusion coefficient, $D_g^{i,eff}$ is corrected for tortuosity and reduction in the open pore space due to presence of liquid water via Bruggeman correlation, *i.e.:*

$$D_g^{i,eff} = \left[\varepsilon(1-s)\right]^{1.5} D_g^i \quad (7)$$

Eq. (4) resembles the single-phase species conservation except for the last term, which describes the capillary transport of species. Note that, unlike the UFT approximation, the capillary transport term also accounts for the variation in gas-phase pressure in the porous media, hence it also considers the gas flow in counter-direction to capillarity-induced gas flow. In the absence of gravity, mass flux of liquid phase, $\vec{j}_l$ is given as:

$$\vec{j}_l = \frac{\lambda_l \lambda_g}{\nu} K \nabla p_c \quad (8)$$

where λ_l and λ_g are relative mobilities of gas and liquid phases, respectively:

$$\lambda_l = \frac{k_{rl}/\nu_l}{k_{rl}/\nu_l + k_{rg}/\nu_g} \qquad \lambda_g = 1 - \lambda_l \quad (9)$$

and ν is the mixture viscosity:

$$\nu = \left(\frac{k_{rl}}{\nu_l} + \frac{k_{rg}}{\nu_g}\right)^{-1} \quad (10)$$

Here, GDLs and MPL are assumed to be isotropic and homogeneous and the relative permeabilities of individual phases are assumed to be proportional to the cube of individual phase saturations, *i.e.*:

$$k_{rk} = s_k^{\,3} \quad (11)$$

Capillary pressure is the difference of the wetting and non-wetting phase pressures, *i.e.*:

$$p_c = p_g - p_l \quad (12)$$

and related to phase saturations via Leverett function, such that:

$$p_c = \sigma \cos(\theta_c) \left(\frac{\varepsilon}{K}\right)^{1/2} J(s) \quad (13)$$

where *J(s)* is the Leverett function, and given for both hydrophobic and hydrophilic GDLs as (Pasaogullari and Wang, 2004b):

$$J(s) = \begin{cases} 1.417(1-s) - 2.120(1-s)^2 + 1.263(1-s)^3 & \text{if } \theta_c < 90° \\ 1.417s - 2.120s^2 + 1.263s^3 & \text{if } \theta_c > 90° \end{cases} \quad (14)$$

Note that for a hydrophilic medium, the wetting phase is the liquid phase, therefore Leverett function is expressed in terms of gas phase saturation, whereas in hydrophobic medium, the gas phase becomes the wetting phase and so the liquid phase saturation is used. Contact angle, θ_c, of the GDL is dependent upon hydrophilic ($0^o < \theta_c < 90^o$) or hydrophobic ($90^o < \theta_c < 180^o$) nature of the GDL, and varies with the Teflon content. Here, the surface tension σ, for liquid water-air system is taken as 0.0625 N/m.

In steady state, the water species conservation equation reduces to:

$$\nabla \cdot \left(\gamma_c^{H_2O} \vec{u} C^{H_2O}\right) = \nabla \cdot \left[D_g^{H_2O,eff} \nabla C_g^{H_2O}\right] - \nabla \cdot \left[\left(\frac{1}{M^{H_2O}} - \frac{C_g^{H_2O}}{\rho_g}\right) \vec{j}_l\right] \quad (15)$$

When integrated along the GDM thickness, the Eq. (15) becomes:

$$\gamma_c^{H_2O} \vec{u} C^{H_2O} - D_g^{H_2O,eff} \nabla C_g^{H_2O} + \left(\frac{1}{M^{H_2O}} - \frac{C_g^{H_2O}}{\rho_g}\right) \vec{j}_l = \vec{j}_w \quad (16)$$

Here, $\vec{j}_w$ represents the net molar flux of water through the individual layers of MEA and has the units of [mol·m^{-2}·s^{-1}]. For each layer, $\vec{j}_w$ is a function of local current density through the production and net water transport coefficient across the membrane. The corresponding expressions for net water flux for each component of MEA is given in Table 1.

The liquid saturation is expressed in terms of the total water concentration via the following relation, based on Eq. (6):

$$s = \frac{C^{H_2O} - C_{sat}^{H_2O}}{\frac{\rho_l}{M^{H_2O}} - C_{sat}^{H_2O}} \quad (17)$$

Once the liquid saturation, *s* is obtained, the individual phase velocities are obtained using the following relations.

$$\rho_l \vec{u}_l = \vec{j}_l + \lambda_l \rho \vec{u} \quad (18)$$

$$\rho_g \vec{u}_g = -\vec{j}_l + \lambda_g \rho \vec{u} \quad (19)$$

Then the phase pressures can be obtained using Darcy's law for each individual phase:

$$\nabla p_k = -\frac{\mu_k}{K} \vec{u}_k \quad (20)$$

Water Transport across the Membrane

In this study, the transport of water across the membrane by electro-osmotic drag due to proton flux, permeation due to hydraulic pressure gradient and diffusion due to concentration gradient are considered. It is known that the electro-osmotic drag of water is linearly proportional to the number of protons transported across the membrane, and this proportionality constant is called "electro-osmotic drag coefficient" and known to be a function of water content of the membrane (Zawodzinski *et al.* 1995). It was shown that the electro-osmotic drag coefficient for Nafion® based membranes is around 2.5 when the membrane is saturated with liquid water and around unity when humidified with water vapor. The three modes of water transport, namely electro-osmotic drag, permeation and diffusion are described with the following equation.

$$\nabla \cdot \left(-\frac{K_{mem}}{\nu_l M^{H_2O}} \nabla p\right) = \nabla \cdot \left(D_m^w \nabla C_m^w\right) - \nabla \cdot \left(n_d \frac{I}{F}\right) \quad (21)$$

where

$$C_m^w = \lambda \frac{\rho_{dry}}{EW} \quad (22)$$

Here, λ is the number of water molecules per sulfonate group in the membrane and defined as the water content of the membrane. The relation of the membrane water content with the surrounding medium is generally given by a water uptake curve. Zawodzinski *et. al.* (1993) measured the water uptake curve for Nafion® membranes, and concluded that the water content of the membrane is around 16 when it is in equilibrium with liquid water at 80ºC and the relation between the water content of the membrane and the surrounding medium water activity (P_{H2O}/P_{sat}) is given by the water uptake curve when the membrane is humidified with water vapor. Here, we use a 3rd order polynomial curve fit to Zawodzinski *et. al.*'s data to calculate membrane water content when membrane is in equilibrium with water vapor. We, then linearly extrapolate the water uptake curve to calculate the water content of the membrane when it is in equilibrium with two-phase mixture of water vapor of activity of *a*=1 and liquid saturation of *s*, as

shown in Figure 2. Therefore, the membrane water content is calculated by:

$$\lambda = \begin{cases} 1.4089 + 11.263a - 18.768a^2 + 16.209a^3 & \\ & \text{if } C^{H_2O} \le C_{sat} \\ 10.1129(1-s) + 16s & \text{if } C^{H_2O} > C_{sat} \end{cases} \quad (23)$$

In Eq. (21), K_{mem} is the membrane hydraulic permeability and n_d is the electro-osmotic drag coefficient. When integrated along the membrane thickness, Eq. (21) becomes:

$$-\frac{K_{mem}}{\nu_l \cdot M^{H_2O}} \nabla p_l - D_m^w \nabla C_m^w + n_d \frac{I}{F} = \vec{j}_w \quad (24)$$

The values reported in the literature for hydraulic permeability of membrane show a great variation. It is reported between $1.8 \cdot 10^{-18}$ m^2 (Bernardi and Verbrugge, 1992) to $2 \cdot 10^{-20}$ m^2 (Meier and Eigenberger, 2004), for Nafion® based membranes humidified with liquid water. In this work, we use the latest available data from Meier and Eigenberger, which is $2 \cdot 10^{-20}$ m^2 for a membrane fully humidified with liquid water at 80ºC (i.e. λ=16).

Here, the diffusion coefficient of water in the membrane is taken from Motupally *et. al.* (2000) and is given as:

$$D_m^w = \begin{cases} 3.1 \cdot 10^{-7} \lambda \left(e^{0.28\lambda} - 1\right) e^{-1346/T} & 0 < \lambda \le 3 \\ 4.17 \cdot 10^{-8} \lambda \left(1 + 161 e^{-\lambda}\right) e^{-1346/T} & 3 \le \lambda < 17 \end{cases} \quad (25)$$

in m^2/s.

Boundary Conditions

In this work, we assume that the gas channels are free of liquid water. Furthermore, gas diffusion media for both anode and cathode are saturated with water vapor; therefore the water concentration at the GDM-gas channel interface is equal to the saturation concentration, therefore the liquid saturation at these interfaces is zero.

$$s(x=0) = s_{A-GC/GDL} = 0 \quad (26)$$

$$s(x=\delta_{MEA}) = s_{C-GC/GDL} = 0 \quad (27)$$

Consequently, the capillary pressures at these interfaces are also zero, and the gas phase pressure is equal to the channel pressure.

$$p_g(x=0) = p_A \quad (28)$$

$$p_g(x=\delta_{MEA}) = p_C \quad (29)$$

Numerical Procedure

The given model is solved for three different regions, namely anode GDL, PEM and cathode GDM, simultaneously. As shown in Table 1, the fluxes are all function of net water transport coefficient, α, which is not known initially. Therefore, an iterative procedure is used to determine α. An initial guess is provided for α, and this guess is improved in consecutive iterations using bisection method until water content of the membrane converges to the given accuracy. A relative error margin of 10^{-7} in water content is set for convergence criteria, which requires around 25 iterations for obtaining α up to 8-digit accuracy. The governing equations of water transport are non-linear ordinary differential equations, which are solved using a 4th order adaptive step Runge-Kutta method.

RESULTS AND DISCUSSION

Effect of Micro-Porous Layer

In order to analyze the effect of MPL on liquid water transport in PEFC, four different GDM configurations are analyzed. These configurations are achieved by varying the anode and cathode GDM. Both of the anode and cathode GDL properties are selected from values of carbon paper. Two of the configurations have hydrophobic GDL in the anode (wet-proofed, θ_c=110º), and the other two have hydrophilic GDL (not wet-proofed, θ_c=70º). In all cases, cathode GDL is wet-proofed and in two of the cases cathode GDL is coated with MPL. The MPL properties used here are taken from the base case, as well as for the analyses in the next sections. The properties of the materials used here are given in Table 2, along with the associated transport parameters.

In Figure 3, the variation of net water transport coefficient with current density is given for all these cases. Note that, net water transport coefficient, α is defined as the number of water molecules transported per proton across the membrane, therefore when α is positive, the net water transport across the membrane is towards cathode.

$$\alpha = \frac{j_{mem}^{H_2O} \cdot F}{I} \quad (30)$$

It is seen that the net water transport coefficient profile does not follow a single trend across the entire current density range. Around α=0, a change in the trend is visible and this is due to the change in the anode water transport phenomena at α=0. When α is less than zero, there is a net water transport towards the anode, and since the anode is already humidified, there is liquid water in the anode GDL and water transport in the anode GDL is governed by the capillary force. However, when α is positive, net water transport across the anode GDL is towards the membrane, and it is governed by the gas phase diffusion of the water vapor, which is much stronger than the capillary transport of water.

It is clearly seen in all cases that, the use of a hydrophilic GDL in anode side decreases the water flux towards anode only when α<0. Here, there are two distinct effects to be considered: In the hydrophilic porous media, the capillary pressure is positive; hence liquid pressure is smaller than gas pressure, creating a larger pressure differential across the membrane, therefore the permeation of water due to hydraulic pressure gradient from cathode to anode is enhanced. However, as shown by Pasaogullari and Wang (2004b), liquid water transport in hydrophilic GDLs is weaker than in hydrophobic GDL. Therefore, with the use of hydrophilic GDL on the anode side, the liquid saturation is increased, which increases the water content of the membrane in the anode side of the membrane, as shown in Eq. (23). Therefore, the water concentration gradient across the membrane is reduced, which decreases the diffusion flux from cathode to anode. When α>0, since the gas diffusion is the only mode of water transport in the anode GDL, no effect of anode GDL wettability is seen.

It is also evident from Figure 3 that the net water transport coefficient increases with increasing current density. In membrane, the electro-osmotic drag of water is in counter-direction to convective and diffusive transport of water. Electro-osmotic drag is towards cathode due to proton flux, and convective and diffusive transport of water is towards anode

since liquid pressure and water content is higher in the cathode side of the membrane than the anode side. Therefore, with increasing current density, the electro-osmotic drag increases and starts to dominate over the convective and diffusive transport of water across the membrane, resulting in increasing net water transport coefficient with increasing current density. When cathode GDL is coated with MPL, it is seen that water transport towards anode is significantly increased and this increase is clearly visible at the entire current density range.

In Figure 4, the liquid pressure profiles in all four configurations are shown at a current density of 0.1 A/cm^2. In this current density, all four configurations result in two-phase transport in both the anode and the cathode GDM. The inset of the figure shows the details of liquid pressure across the membrane. As stated above, the liquid pressure differential across the membrane is higher when anode GDL is hydrophilic. However, this difference becomes less significant when cathode GDL is coated with MPL. Due to its smaller pore size, MPL has much smaller permeability; therefore, liquid water flow requires higher pressure differential across the MPL, increasing liquid pressure on the cathode side of the membrane. Here, the permeability of MPL is calculated from the following expression given by Rumpf and Gutte (Kaviany, 1995) for packed beds with narrow range of distribution in size:

$$K = \frac{\varepsilon^{5.5}}{5.6} d^2 \tag{31}$$

where d is the average pore diameter. For an MPL of mean pore size of 1 μm and porosity of 0.5, this expression gives a permeability of $3.95 \cdot 10^{-15}$ m^2, which is comparable with experimentally measured values.

Figure 5 shows the liquid saturation profiles in anode and cathode GDM at the same current density. It is seen that the liquid saturation in cathode GDL is decreased by use of an MPL due to decreased cathode water flux. It is also seen in cathode GDM, there is a discontinuity in the liquid saturation profile at the GDL-MPL interface. This discontinuity is governed by the continuity of phase pressures at this interface. Since both gas and liquid pressures are continuous at this interface, the capillary pressure is also continuous. Following the definition of capillary pressure in Eq. (13), one has the following relation for pressure continuity at the GDL-MPL interface.

$$\cos\left(\theta_c{}^{\mathrm{GDL}}\right)\left(\frac{\varepsilon^{\mathrm{GDL}}}{K^{\mathrm{GDL}}}\right)^{1/2} J\left(s_{\mathrm{int}}^{\mathrm{GDL}}\right) = \cos\left(\theta_c{}^{\mathrm{MPL}}\right)\left(\frac{\varepsilon^{\mathrm{MPL}}}{K^{\mathrm{MPL}}}\right)^{1/2} J\left(s_{\mathrm{int}}^{\mathrm{MPL}}\right) \tag{32}$$

It is clear that this discontinuity is a function of wetting and porous characteristics of MPL and GDL, as well as the liquid flux in the cathode. Due to this discontinuity, liquid saturation in cathode catalyst layer-GDM interface may also be smaller than single-layer configurations depending on the micro-structure of MPL; therefore catalyst layer flooding can also be reduced with MPL.

It is also seen from Figure 5 that when hydrophilic GDL is used in anode, the liquid saturation in the anode GDL increases, which is particularly due to smaller capillarity effects in hydrophilic GDL. It has been shown that capillary water transport is stronger in hydrophobic GDLs than hydrophilic GDLs, particularly at lower liquid saturations (Pasaogullari and Wang, 2004).

Similar water transport characteristics that are observed with MPLs can also be achieved by adjusting the operating conditions, such as using higher cathode and lower anode pressures. Particularly, operating with pressure differentials has been shown to significantly improve the performance (Voss *et al.*, 1995, Jannsen and Overvelde, 2001, Beattie *et al.* 1999). In all these examples, an increased pressure differential across the membrane is formed to enhance the back-flux (*i.e.* towards anode) of water, similar to what MPL causes.

Effect of MPL Thickness

The effect of the thickness of the MPL is analyzed using the model explained in the earlier sections. The parameters used for this case are the same as in Table 2, except that the thickness of the MPL is varied between 10 μm and 50 μm. As seen in Figure 6, the net water transport coefficient is a strong function of MPL thickness. As the MPL thickness increases, the net water transport coefficient curve shifts downwards indicating that the water flux towards the anode is increasing. With increasing MPL thickness, the resistance to liquid water flow in the cathode GDM increases, and this increased resistance causes the fraction of water transported through the membrane towards anode to increase, hence results in a decrease in cathode water flux. Inset of the Figure 6 shows the change of net water transport coefficient with MPL thickness at several current densities. It is seen that the thickness of the MPL is particularly effective at lower current densities due to smaller electro-osmotic drag flux.

Effect of Mean Pore Size of MPL

Figure 7 shows the net water transport coefficient across the membrane for different mean pore sizes of MPL. Here, the properties of the MPL are taken from the base case, which are given in Table 2 except for the mean pore size. The net water transport curve shifts downwards with decreasing mean pore size, indicating increasing water flux towards anode. The permeability of MPL decreases with the pore size (see Eq. (31)), which increases the resistance to water flow towards cathode channel. Therefore, water tends to flow in the path which has smaller resistance, which in turn increases the flow rate towards anode. This effect obviously is much more visible in lower current densities, where back-flux of water is dominating over the electro-osmotic drag. As the current density increases, the electro-osmotic drag of water across the membrane becomes larger, diminishing the effect of MPL. As seen in the inset of Figure 7, the effect of the mean pore size of MPL starts to disappear for larger pore sizes as the MPL permeability becomes closer to GDL permeability. As the absolute permeability is directly proportional to the square of the mean pore size (Eq. (31)), liquid pressure differential across the MPL is magnified with decreasing pore size. This increase in the MPL pressure differential causes a higher pressure differential across the membrane, causing higher back-flux of water towards anode.

It is evident that smaller pore size in MPL is increasing the tendency of liquid water flow towards anode. However, smallest pore size is probably not the optimal design, thus the gas phase transport will be hampered with the decreasing pore sizes. The gas-phase transport is most likely to be in the Knudsen regime in MPL due to the much smaller pore sizes. In Knudsen regime, the wall-to-molecule interactions dominates over the molecule-to-molecule interactions, and the pore size becomes the most important factor for gas diffusion. On the

other hand, in the larger pore scales, where binary diffusion of gases dominates, the bulk porosity of the porous media becomes the dominating structural parameter. Therefore, the optimal design of the MPL pore size will be governed by the competing effects of liquid water transport and oxygen diffusion.

Effect of MPL bulk porosity

Figure 8 shows the net water transport coefficient with respect to current density for different bulk porosities of MPL. As seen in Figure 8, bulk porosity of the MPL is also quite effective in governing the water transport in PEFC. With the decreasing bulk porosity of MPL, the resistance to the liquid water flow in the cathode increases, which results in increased water flux towards anode, as indicated by downward shift in the net water transport curve in Figure 8. The inset of the Figure 8 shows the change in the net water transport with porosity at different current densities, and it is clearly seen that the effect of MPL porosity is more dominant at lower current densities, since electro-osmotic drag is not dominating at these current densities. The behavior shows great similarities to the effect of MPL pore diameter, which governs the absolute permeability. As seen in Eq. (13) absolute permeability and the bulk porosity has the same effect on the water transport. The pressure differential across the MPL increases as the resistance to liquid water flow on the cathode increases, which results in higher liquid pressure differential across the membrane, consequently increasing liquid flow towards anode.

Effect of MPL Wettability

As with the porosity and the pore diameter, the wetting characteristics of the MPL also affect the water transport in the PEFC. Capillarity is a direct function of wettability of the porous media. In this work, we characterize the wettability of MPL with an average contact angle, and the effect of this average contact angle is analyzed. Figure 9 shows the net water transport coefficient for different contact angles of MPL. It is seen that as the contact angle of the MPL is getting smaller, net water transport towards anode is increased. It is evident from Eq. (12) that the capillary pressure is a linear function of $\cos(\theta_c)$. When the MPL is less hydrophobic (*i.e.* lower contact angle), the liquid pressure build-up in the MPL is higher, resulting in a higher liquid pressure at the cathode side of the membrane. Consequently, the water flux towards anode is higher.

In this work, we haven't accounted for the fact that the mean pore size varies with the wettability of MPL. The PTFE and carbon particles used in MPL construction have significantly different sizes; hence the mean pore size of the MPL changes with the wettability. This effect has to be also accounted for accurate analysis and optimization of MPL. However, in general it can be said that the MPL provides better water management capabilities with increasing hydrophobicity due to decreased cathode flooding.

CONCLUSIONS

A one-dimensional two-phase model developed for the entire MEA sandwich of PEFCs and the effects of MPL and MPL properties on water transport are analyzed. The following conclusions are drawn from this study:

*(i)*Multi-layered cathode gas diffusion media provides better water management characteristics, particularly by increasing the tendency of water flow towards anode. This results from the increase in the resistance to liquid water flow in the cathode, which then provides a higher pressure differential across the membrane increasing the hydraulic permeation of water across the membrane.

*(ii)*The reduced water flow towards cathode decreases the cathode flooding; therefore it improves the cell performance by decreasing the mass transfer limitations. Furthermore, due to the different micro-porous and wetting characteristics of MPL and GDL, there is a discontinuity in cathode liquid saturation profile, which consequently reduces the flooding in cathode catalyst layer/MPL interface.

*(iii)*It is seen that the water flux towards anode increases with smaller pore size, porosity and contact angle and larger thickness of the MPL. Although, these abovementioned properties improve the water management, they're most likely not the properties of the optimal MPL design. The gas phase transport of oxygen and electron transport is also affected by the MPL structure and they also have to be accounted for an MPL optimization study. Our current work focuses on analyzing these effects in order to optimize the MPL structure.

ACKNOWLEDGEMENTS

Funding for this work from Sandia National Laboratories is gratefully acknowledged.

REFERENCES

Beattie, P.D., Basura, V.I. and Holdcroft, S., 1999, "Temperature and pressure dependence of O_2 reduction at Pt/Nafion 117 and Pt/BAM 407 interfaces," *J. Electroanal. Chem.*, Vol. 468, pp. 180-192.

Bernardi, D.M. and Verbrugge, M.W., 1992, "A Mathematical Model of the Solid-Polymer Electrolyte Fuel Cell," *J. Electrochem. Soc.*, Vol. 139, pp. 2477-2491.

He, W., Yi, J.S. and Nguyen, T.V., 2000, "Two-phase flow model of the cathode of PEM fuel cells using interdigitated flow fields" *AIChE J.*, Vol. 46, pp. 2053-2064.

Janssen, G.J.M. and Overvelde, M.L.J., 2001, "Water transport in the proton-exchange-membrane fuel cell: Measurements of the effective drag coefficient," *J. Power Sources*, Vol. 101, pp. 117-125.

Kaviany, M., 1995, *Principles of Heat Transfer in Porous Media*, 2nd Edition, Springer-Verlag, New York.

Kong, C.S., Kim, D-Y., Lee, H-K., Shul, Y-G. and Lee, T-H., 2002, "Influence of pore-size distribution of diffusion layer on mass-transport problems of proton exchange membrane fuel cells," *J. Power Sources*, Vol. 108, pp. 185-191.

Meier, F. and Eigenberger, G., 2004, "Transport parameters for the modelling of water transport in ionomer membranes for PEM-fuel cells," *Electrochim. Acta*, Vol. 49, pp. 1731-1742.

Motupally, S., Becker, J.A. and Weidner, J.W., "Diffusion of water in Nafion 115 membranes," *J. Electrochem. Soc.*, Vol. 147, pp. 3171-3177.

Nam, J-H. and Kaviany, M., 2003, "Effective diffusivity

and water-saturation distribution in single- and two-layer PEMFC diffusion medium," *Int. J. Heat and Mass Tr.*, Vol. 46, 4595-4611.

Pasaogullari, U. and Wang, C.Y., 2004, Two-Phase Transport and the Role of Micro-Porous Layer in Polymer Electrolyte Fuel Cells," *Electrochim. Acta*, Vol. 49, 4359-4369.

Pasaogullari, U. and Wang, C.Y., 2004, "Liquid Water Transport in Gas Diffusion Layer of Polymer Electrolyte Fuel Cells," *J. Electrochem. Soc.*, Vol. 151, pp. A399-A406.

Pasaogullari, U. and Wang, C.Y., 2004, "Two-Phase Modeling and Flooding Prediction of Polymer Electrolyte Fuel Cells," *J. Electrochem. Soc.*, in press.

Qi, Z. and Kaufman, A., 2002, "Improvement of water management by a microporous sublayer for PEM fuel cells," *J. Power Sources*, Vol. 109, pp. 38-46.

Springer, T.E., Wilson, M.S., and Gottesfeld, S., 1991, "Polymer Electrolyte Fuel Cell Model", J. Electrochem. Soc., Vol. 136, pp. 2334-2342.

Voss, H.H., Wilkinson, D.P., Pickup, P.G., Johnson, M.C. and Basura, V. 1995, "Anode water removal: a water management and diagnostic technique for solid polymer fuel cells," *Electrochim. Acta*, Vol. 40, pp. 321-328.

Wang, C.Y. and Cheng, P., 1997, "Multiphase Flow and Heat Transfer in Porous Media," *Advances in Heat Transfer*, Vol. 30. pp. 93-196.

Weber, A. and Newman, J., Abstract Nr: 1038 204th Electrochemical Society Meeting, October 12-16, 2003, Orlando, Florida.

Wilson, M.S., Valerio, J.A. and Gottesfeld, S., 1995, "Low platinum loading electrodes for polymer electrolyte fuel cells fabricated using thermoplastic ionomers," *Electrochim. Acta*, Vol. 40, pp. 355-363.

Zawodzisnki, T.A., Springer, T.E., Uribe, F. and Gottesfeld S., 1993, "Characterization of polymer electrolytes for fuel cell applications," *Solid State Ionics*, Vol. 60, pp. 199-211.

Zawodzisnki, T.A., Davey, J., Valerio, J. and Gottesfeld S., 1995, "The water content dependence of electro-osmotic drag in proton-conduting polymer electrolytes," *Electrochim. Acta*, Vol. 40, pp. 297-302.

Table 1 Mass and water flux for individual layers of PEFC

	Mass Flux, j_m	**Water Flux, j_w**
Anode GDL	$\frac{I}{F}\left(\frac{M^{H_2}}{2}+\alpha M^{H_2O}\right)$	$\frac{I}{F}\alpha$
Membrane	N/A	$\frac{I}{F}\alpha$
Cathode GDL/MPL	$\frac{I}{F}\left[-\frac{M^{O_2}}{4}+\left(\alpha+\frac{1}{2}\right)M^{H_2O}\right]$	$\frac{I}{F}\left(\alpha+\frac{1}{2}\right)$

Table 2 Material properties, transport parameters and operating conditions

Parameter	**Value**
Transport parameters	
Surface tension, σ	0.0625 N/m
Anode gas kinematic viscosity, $\nu_{g,a}$	4.45×10^{-5} m^2/s
Cathode gas kinematic viscosity, $\nu_{g,c}$	1.78×10^{-5} m^2/s
Liquid kinematic viscosity, ν_l	3.52×10^{-7} m^2/s
Liquid density, ρ_l	974.85 kg/m^3
Material properties	
GDL absolute permeability, K_{GDL}	8.7×10^{-12} m^2
GDL porosity, ε_{GDL}	0.7
Hydrophobic GDL contact angle, θ_c	110º
Hydrophilic GDL contact angle, θ_c	70º
Anode GDL thickness, δ_{AGDL}	300 μm
Cathode gas diffusion medium thickness, δ_C	300 μm
Membrane thickness (Nafion® 112), δ_{mem}	50.8 μm
Membrane hydraulic permeability, K_{mem}	2×10^{-20} m^2
Base case MPL properties	
Thickness, δ_{MPL}	30 μm
Porosity, ε_{MPL}	0.5
Average pore size, d_{MPL}	1000 nm
Absolute permeability, K_{MPL}	3.95×10^{-15} m^2
Contact angle, $(\theta_c)_{MPL}$	120º
Operating Conditions	
Cell temperature, T	353.15 K
Anode channel pressure, p_A	1.5 atm
Cathode channel pressure, p_C	1.5 atm

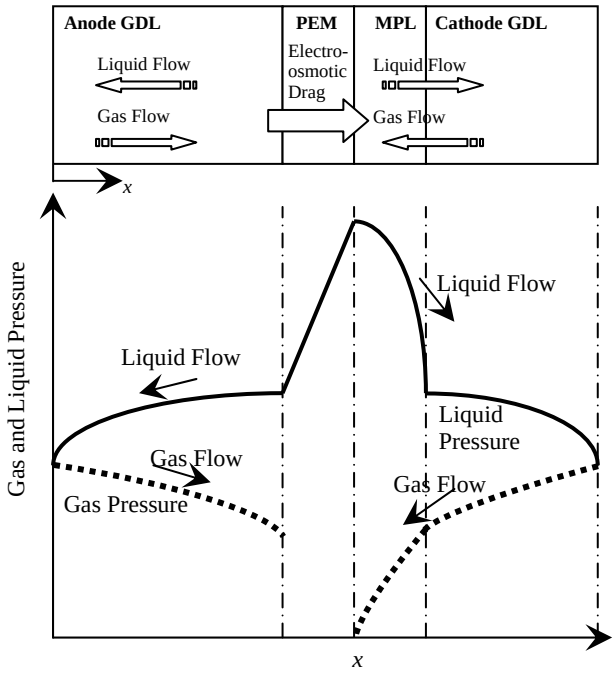

Figure 1 Schematics of modeling domain, transport phenomena and individual phase pressure profiles in PEFCs with micro-porous layers

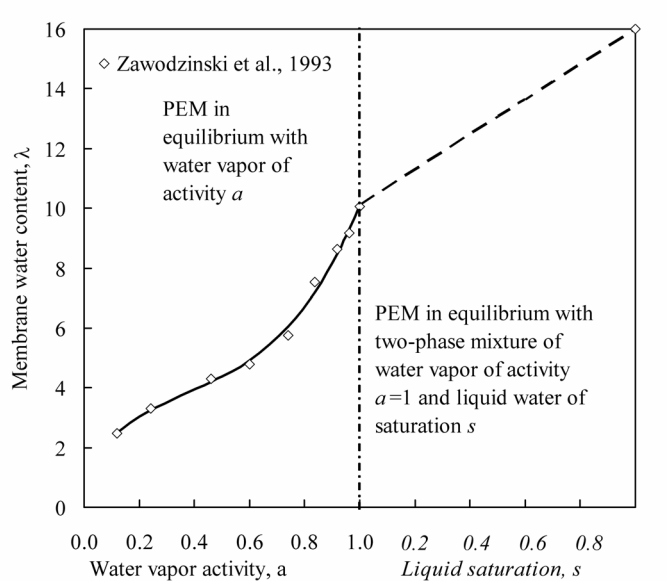

Figure 2 Membrane water uptake. Symbols are experimental measurements of Zawodzinski *et al.* for Nafion® membranes at 80ºC.

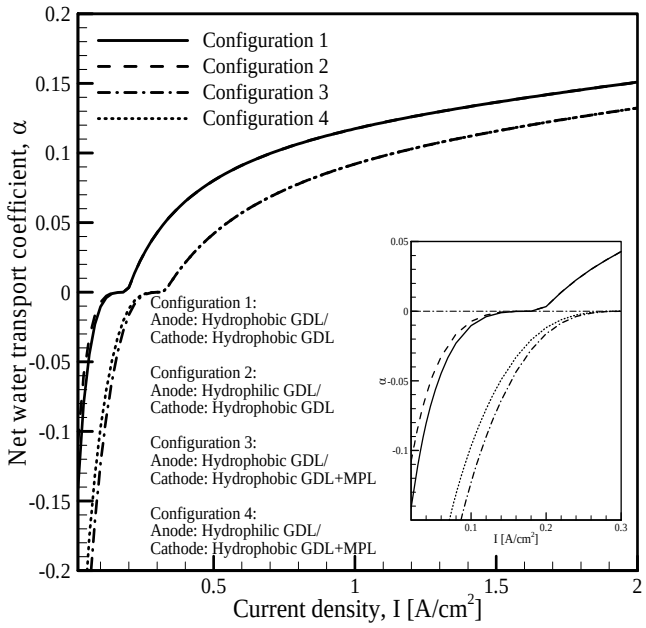

Figure 3 Net water transport coefficient, α for different GDM configurations. MPL properties are taken from base case given in Table 2. Inset shows the enlarged view at lower current densities.

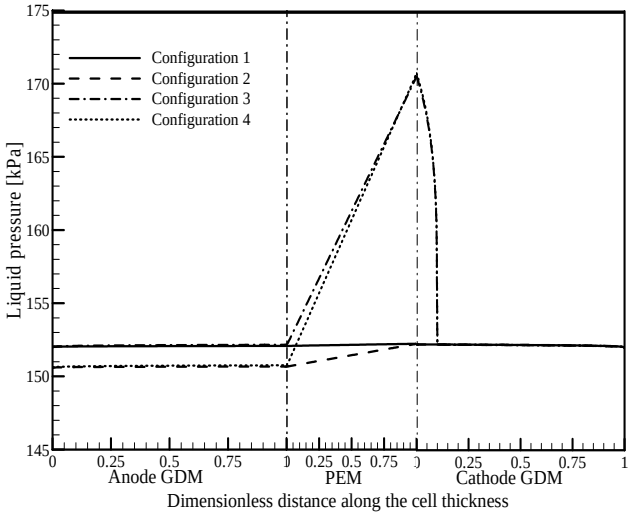

Figure 4 Liquid pressure profiles across the cell thickness for different GDM configurations at 1.5 A/cm^2. For configuration and material properties, refer to Figure 2. Inset shows the details of liquid pressure across the membrane.

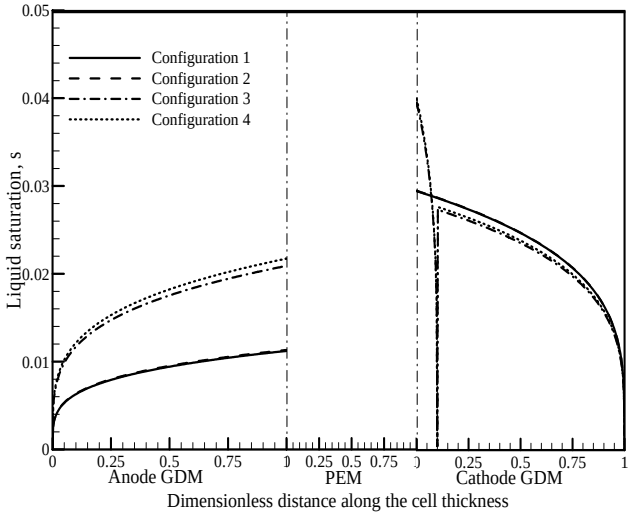

Figure 5 Liquid saturation profiles across the GDM/MEA thickness for different MEA thickness at 1.5 A/cm^2. The configuration details are given in Figure 2.

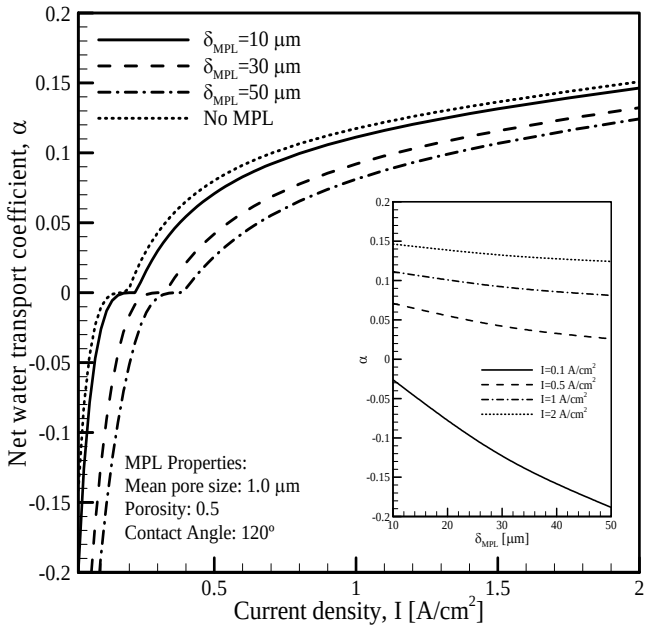

Figure 6 Net water transport coefficient, α for different MPL thicknesses. The rest of the MPL properties are taken from base case given in Table 2. Inset shows the variation of net water transport coefficient with MPL thickness at different current densities.

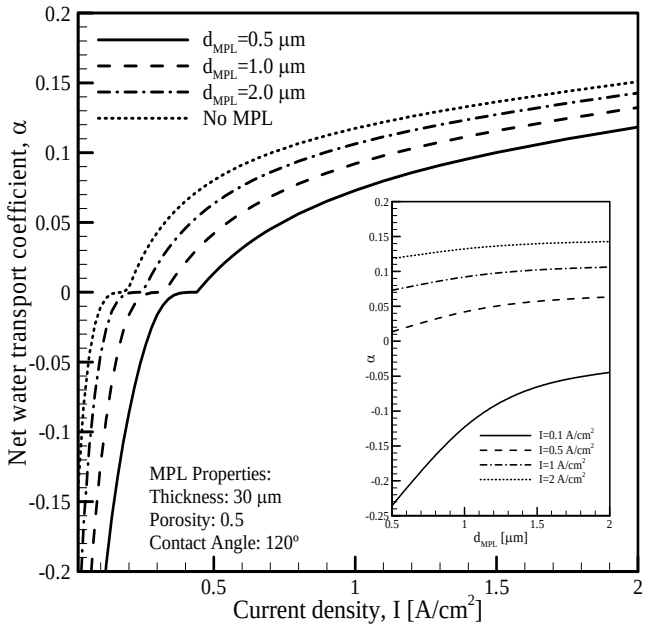

Figure 7 Net water transport coefficient, α for different mean pore sizes of MPL. The rest of the MPL properties are taken from base case given in Table 2. Inset shows the variation of net water transport coefficient with mean pore size of MPL at different current densities.

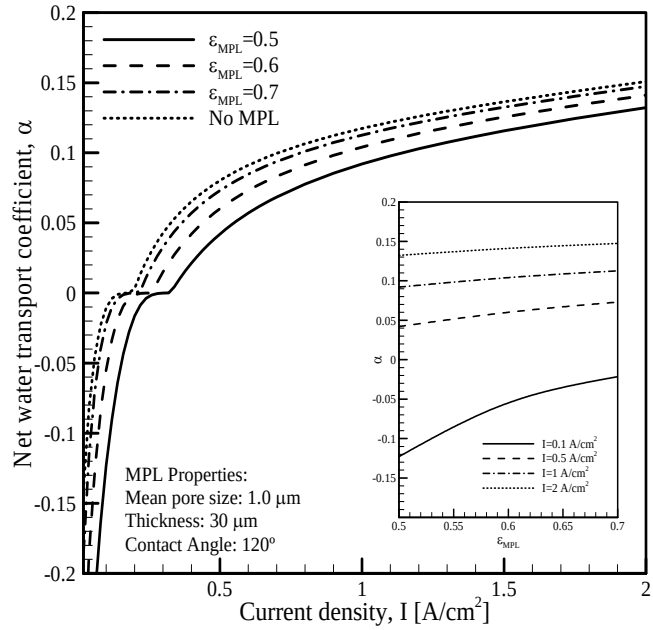

Figure 8 Net water transport coefficient, α for different MPL bulk porosities. The rest of the MPL properties are taken from base case given in Table 2. Inset shows the variation of net water transport coefficient with MPL bulk porosity at different current densities.

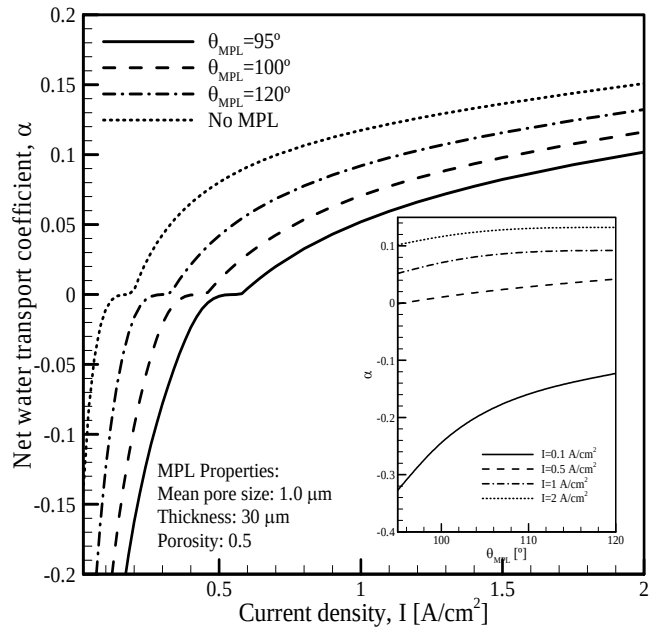

Figure 9 Net water transport coefficient, α for different MPL contact angles. The rest of the MPL properties are taken from base case given in Table 2. Inset shows the variation of net water transport coefficient with MPL contact angles at different current densities.